Long-term stabilization of high power optical parametric chirped-pulse amplifiers

R. Riedel,[1,2,*] M. Schulz,[1,2,3] M. J. Prandolini,[1,3] A. Hage,[3,4] H. Höppner,[3] T. Gottschall,[6] J. Limpert,[1,6] M. Drescher,[2,5] and F. Tavella[1,3]

[1]*Helmholtz-Institut Jena, Fröbelstieg 3, D-07743 Jena, Germany*
[2]*Universität Hamburg, Luruper Chaussee 149, D-22761 Hamburg, Germany*
[3]*Deutsches Elektronensynchrotron DESY, Notkestrasse 85, D-22607 Hamburg, Germany*
[4]*Queens University Belfast, University Road Belfast, BT7 1NN, United Kingdom*
[5]*Center for Free Electron Laser Science, Luruper Chaussee 149, D-22761 Hamburg, Germany*
[6]*Friedrich-Schiller-Universität Jena, Abbe Center of Photonics, Institute of Applied Physics, Albert-Einstein-Str. 15, D-07745 Jena, Germany*

[*]*robert.riedel@desy.de*

Abstract: The long-term stability of optical parametric chirped-pulse amplifiers is hindered by thermal path length drifts affecting the temporal pump-to-signal overlap. A kilowatt-pumped burst amplifier is presented delivering broadband 1.4 mJ pulses with a spectral bandwidth supporting sub-7 fs pulse duration. Active temporal overlap control can be achieved by feedback of optical timing signals from cross-correlation or spectral measurements. Using a balanced optical cross-correlator, we achieve a pump-to-signal synchronization with a residual jitter of only (46 ± 2) fs rms. Additionally, we propose passive pump-to-signal stabilization with an intrinsic jitter of (7.0 ± 0.5) fs rms using white-light continuum generation.

OCIS codes: (140.0140) Lasers and laser optics; (140.3425) Laser stabilization; (190.4410) Nonlinear optics, parametric processes.

References and links

1. F.X. Kärtner, *Few-cycle Laser Pulse Generation and its Applications.* ed. (Springer Verlag, 2004).
2. R. Riedel, A. Al-Shemmary, M. Gensch, T. Golz, M. Harmand, N. Medvedev, M.J. Prandolini, K. Sokolowski-Tinten, S. Toleikis, U. Wegner, B. Ziaja, N. Stojanovic, and F. Tavella, "Single-shot pulse duration monitor for extreme ultraviolet and X-ray free-electron lasers," Nat. Commun. **4**, 1731 (2013)
3. B. W. J. McNeil and N. R. Thomson, "X-ray free-electron lasers," Nat. Photonics **4**, 814-821 (2010)
4. A. M. March, A. Stickrath, G. Doumy, E. P. Kanter, B. Krässing, S. H. Southworth, K. Attenkofer, C. A. Kurtz, L. X. Chen, and L. Young, "Development of high-repetition-rate laser pump/x-ray probe methodologies for synchrotron facilities," Rev. Sci. Instrum. **82**, 073110 (2011)
5. G. Sansone, F. Kelkensberg, J. F. Prez-Torres, F. Morales, M. F. Kling, W. Siu, O. Ghafur, P. Johnsson, M. Swoboda, E. Benedetti, F. Ferrari, F. Lpine, J. L. Sanz-Vicario, S. Zherebtsov, I. Znakovskaya, A. LHuillier, M. Yu. Ivanov, M. Nisoli, F. Martin, and M. J. J. Vrakking, "Electron localization following attosecond molecular photoionization," Nature **465**, 763–766 (2010)
6. X. Zhang, E. Schneider, G. Taft, H. Kaptyen, M. Murnane, and S. Backus, "Multi-microjoule, MHz repetition rate Ti:sapphire ultrafast regenerative amplifier system," Opt. Express **20**, 7015–7021 (2012)
7. A. Dubietis, G. Jonusauskas, and A. Piskarskas, "Powerful femtosecond pulse generation by chirped and stretched pulse parametric amplification in BBO crystal," Opt. Commun. **88**, 437–440 (1992)
8. I. N. Ross, P. Matousek, M. Towrie, A. J. Langley, and J. L. Collier, "The prospects for ultrashort pulse duration and ultrahigh intensity using optical parametric chirped pulse amplifiers," Opt. Commun. **144**, 125-133 (1997)

#193989 - $15.00 USD Received 17 Jul 2013; revised 17 Sep 2013; accepted 2 Oct 2013; published 15 Nov 2013

9. G. Cerullo and S. De Silvestri, "Ultrafast optical parametric amplifiers," Rev. Sci. Instrum. **74**, doi: 10.1063/1.1523642 (2003)
10. J. Rothhardt, S. Hädrich, E. Seise, M. Krebs, F. Tavella, A. Willner, S. Düsterer, H. Schlarb, J. Feldhaus, J. Limpert, J. Rossbach, and A. Tünnermann, "High average and peak power few-cycle laser pulses delivered by fiber pumped OPCPA system," Opt. Express **18**, 12719–12726 (2010)
11. J. Rothhardt, S. Demmler, S. Hädrich, J. Limpert, and A. Tünnermann, "Octave-spanning OPCPA system delivering CEP-stable few-cycle pulses and 22 W of average power at 1 MHz repetition rate,", Opt. Express **20**, 10870–10878 (2012)
12. P. Russbueldt, T. Mans, G. Rotarius, J. Weitenberg, H. D. Hoffmann, and R. Poprawe, "400W Yb:YAG Innoslab fs-Amplifier," Opt. Express **19**, 12230-12245 (2009)
13. P. Russbueldt, T. Mans, J. Weitenberg, H. D. Hoffmann, and R. Poprawe, "Compact diode-pumped 1.1 kW Yb:YAG Innoslab femtosecond amplifier," Opt. Lett. **35**, 4169–4171 (2010)
14. M. Schulz, R. Riedel, A. Willner, T. Mans, C. Schnitzler, P. Russbueldt, J. Dolkemeyer, E. Seise, T. Gottschall, S. Haedrich, S. Duesterer, H. Schlarb, J. Feldhaus, J. Limpert, B. Faatz, A. Tuennermann, J. Rossbach, M. Drescher, and F. Tavella, "Yb:YAG Innoslab amplifier: efficient high repetition rate subpicosecond pumping system for optical parametric chirped pulse amplification," Opt. Lett. **36**, 2456–2458 (2011)
15. M. Schulz, R. Riedel, A. Willner, S. Düsterer, M. J. Prandolini, J. Feldhaus, B. Faatz, J. Rossbach, M. Drescher, and F. Tavella, "Pulsed operation of a high average power Yb:YAG thin-disk multipass amplifier," Opt. Expr. **20** 5038–5043 (2012)
16. G. Mourou and T. Tajima. "The extreme light infrastructure: Optics next horizon," Optics and Photonics News **22**, 47-51 (2011).
17. C. Y. Teisset, N. Ishii, T. Fuji, T. Metzger, S. Köhler, R. Holzwarth, A. Baltŭska, A. M. Zheltikov, and F. Krausz, "Optical Synchronization for OPCPA Chains," Ultrafast Optics V, Springer Series in Optical Sciences **132**, 535–545 (2007)
18. I. Ahmad, S. A. Trushin, Z. Major, C. Wandt, S. Klingebiel, T.-J. Wang, V. Pervak, A. Popp, M. Siebold, F. Krausz, and S. Karsch, "Frontend light source for short-pulse pumped OPCPA system," Appl. Phys. B: Lasers Opt. **97**, 529–536 (2009)
19. H. Fattahi, C. Y. Teisset, O. Pronin, A. Sugita, R. Graf, V. Pervak, X. Gu, T. Metzger, Z. Major, F. Krausz, and A. Apolonski "Pump-seed synchronization for MHz repetition rate, high-power optical parametric chirped pulse amplification," Opt. Express **20**, 9833–9840 (2012)
20. A. Schwarz, M. Ueffing, Y. Deng, X. Gu, H. Fattahi, T. Metzger, M. Ossiander, F. Krausz, and R. Kienberger, "Active stabilization for optically synchronized optical parametric chirped pulse amplification," Opt. Express **20**, 5557–5565 (2012)
21. K. Tiedtke, A. Azima, N. von Bargen, L. Bittner, S. Bonfigt, S. Düsterer, B. Faatz, U. Frühling, M. Gensch, Ch. Gerth, N. Guerassimova, U. Hahn, T. Hans, M. Hesse, K. Honkavaar, U. Jastrow, P. Juranic, S. Kapitzki, B. Keitel, T. Kracht, M. Kuhlmann, W. B. Li, M. Martins, T. Nez, E. Plnjes, H. Redlin, E. L. Saldin, E. A. Schneidmiller, J. R. Schneider, S. Schreiber, N. Stojanovic, F. Tavella, S. Toleikis, R. Treusch, H. Weigelt, M. Wellhfer, H. Wabnitz, M. V. Yurkov, and J. Feldhaus, "The soft x-ray free-electron laser FLASH at DESY: beamlines, diagnostics and end-stations," New J. Phys. **11**, 023029 (2009)
22. G. Lambert, T. Hara, D. Garzella, T. Tanikawa, M. Labat, B. Carre, H. Kitamura, T. Shintake, M. Bougeard, S. Inoue, Y. Tanaka, P. Salieres, H. Merdj, O. Chubar, O. Gobert, K. Tahara, and M.-E. Couprie, "Injection of harmonics generated in gas in a free-electron laser providing intense and coherent extreme-ultraviolet light", Nat. Phys. **2**, 296–300 (2008)
23. B. Faatz, N. Baboi, V. Ayvazyan, V. Balandin, W. Decking, S. Düsterer, H.-J. Eckoldt, J. Feldhaus, N. Golubeva, K. Honkavaara, M. Körfer, T. Laarmann, A. Leuschner, L. Lilje, T. Limberg, D. Nölle, F. Obier, A. Petrov, E. Plönjes, K. Rehlich, H. Schlarb, B. Schmidt, M. Schmitz, S. Schreiber, H. Schulte-Schrepping, J. Spengler, M. Staack, F. Tavella, K. Tiedtke, M. Tischer, R. Treusch, M. Vogt, A. Willner, J. Bahrdt, R. Follath, M. Gensch, K. Holldack, A. Meseck, R. Mitzner, M. Drescher, V. Miltchev, J. Rönsch-Schulenburg, and J. Rossbach, "Flash II: Perspectives and challenges," Nucl. Instr. Meth. A **635(1)**, S2–S5 (2011)
24. A. Höll, Th. Bornath, L. Cao, T. Döppner, S. Düsterer, E. Förster, C. Fortmann, S. H. Glenzerd, G. Gregorie, T. Laarmann, K.-H. Meiwes-Broer, A. Przystawik, P. Radcliffe, R. Redmer, H. Reinholz, G. Röpke, R. Thiele, J. Tiggesbäumker, S. Toleikis, N. X. Truong, T. Tschentscher, I. Uschmann, and U. Zastrau, "Thomson scattering from near-solid density plasmas using soft X-ray free electron lasers," High. Energ. Dens. Phys. **3**, 120–130 (2007)
25. T. R. Schibli, J. Kim, O. Kuzucu, J. T. Gopinath, S. N. Tandon, G. S. Petrich, L. A. Kolodziejski, J. G. Fujimoto, E. P. Ippen, and F. X. Kaerntner, "Attosecond active synchronization of passively mode-locked lasers by balanced cross correlation", Opt. Lett. **28**, 947–949 (2003)
26. M. Bradler, P. Baum, and E. Riedle, "Femtosecond continuum generation in bulk laser host materials with sub-μJ pump pulses," Appl. Phys. B: Lasers Opt. **97**, 561–574 (2009)
27. Moritz Emons, Andy Steinmann, Thomas Binhammer, Guido Palmer, Marcel Schultze, and Uwe Morgner, "Sub-10-fs pulses from a MHz-NOPA with pulse energies of 0.4 μJ, "Opt. Express **18**, 1191-1196 (2010)
28. J. Jiang, Z. Zhang, and T. Hasama, "Evaluation of chirped-pulse-amplification systems with Offner triplet tele-

#193989 - $15.00 USD Received 17 Jul 2013; revised 17 Sep 2013; accepted 2 Oct 2013; published 15 Nov 2013

scope stretchers, J. Opt. Soc. Am. B **19**, 678–683 (2002)
29. F. Tavella, A. Marcinkevicius, and F. Krausz, "Investigation of the superfluorescence and signal amplification in an ultrabroadband multiterawatt optical parametric chirped pulse amplifier system," New. J. Phys. **8**, 219 (2006)
30. S. Demmler, J. Rothhardt, S. Hädrich, J. Bromage, J. Limpert, and A. Tünnermann, "Control of nonlinear spectral phase induced by ultrabroadband optical parametric amplification," Opt. Lett. **37**, 3933–3935 (2012)
31. S. Hädrich, J. Rothhardt, M. Krebs, S. Demmler, J. Limpert, and A. Tünnermann, "Improving carrier-envelope phase stability in optical parametric chirped-pulse amplifiers by control of timing jitter," Opt. Lett. **37**, 4910–4912 (2012)
32. A. Brodeur and S. L. Chin, "Ultrafast white-light continuum generation and self-focusing in transparent condensed media," J. Opt. Soc. Am. B **16**, 637–650 (1999)
33. Z. Wu, H. Jiang, Q. Sun, H. Yand, and Q. Gong, "Filamentation and temporal reshaping of a femtosecond pulse in fused silica," Phys. Rev. A **68**, 063820 (2003)

1. Introduction and Overview

The generation and control of ultrashort laser pulses are of vital importance in the field of ultrafast dynamics of matter on femtosecond timescales [1, 2]. The advancement of X-ray free-electron lasers (FELs) extends this even towards the atomic scale [3]. X-ray and optical pump-probe experimental techniques profit from an increased repetition rate on both the FEL and the optical laser side [4]. Experiments investigating weak light-matter interactions would tremendously benefit in terms of data quality and statistical relevance. For example, studies of dissociative ionization fragments using table-top soft x-ray sources require high intensities at high repetition rates [5]. Meanwhile, FELs provide MHz repetition rates at pulse energies of hundreds of µJ, whereas ultrashort optical laser amplifiers hardly reach the few-µJ regime at these repetition rates. Available titanium sapphire (Ti:Sa) chirped-pulse amplifiers (CPA) require sophisticated cooling technology to reach a few µJ at MHz repetition rates [6]. In contrast, non-collinear optical parametric chirped-pulse amplifiers (OPCPA) [7–9] are scalable to hundreds of watts and feature an almost octave-spanning gain bandwidth. Recently demonstrated fiber pumped OPCPAs deliver ultrashort few-cycle pulses at average powers of tens of watts [10, 11]. To further increase the output power of such OPCPA systems, the development of kW-level solid-state pump amplifiers with sub-picosecond to few-picosecond pulse durations is required. This can be achieved by Innoslab [12–14] and thin-disk amplifier technology [15]. With these devices available, the development of a high repetition-rate OPCPA at the Extreme Light Infrastructure, Attosecond Light Pulse Source (ELI ALPS) is planned [16]. In the first project phase, this system is aiming at delivering few-cycle pulses at 100 W average power (1 mJ at 100 kHz repetition rate) to provide attosecond pulses at unprecedented average photon flux. However, with ultrashort pump pulses in the picosecond range a major technological challenge arises, because the OPCPA output stability is highly sensitive to the temporal overlap between pump and signal pulses within the amplifier crystals. All-optical synchronization of the pump and signal pulses was introduced in order to avoid additional active electronic synchronization of two master oscillators [17–19]. However, the remaining thermal path length drift in the pump CPA causes instabilities on the long-term scale within tens of seconds to minutes [20].

A high power burst-mode OPCPA is under developement at the FEL FLASH [21]. The key parameters are given by the accelerator itself and the experimental requirements for pump-probe and seeding experiments [22, 23]. Important accelerator parameters are the burst duration of 800 µs and the burst repetition rate of 10 Hz. Each 800 µs electron bunch train generates up to 800 brilliant ultrashort XUV pulses. For the application at FLASH, the high power OPCPA should also operate at up to 1 MHz. The experimental requirements for the pulse energy and the pulse duration are 1 mJ and sub-7 fs, respectively. The short pulse durations enhance the temporal resolution of pump-probe experiments that use equivalently short XUV pulses provided by FLASH. Optical peak powers of $P_{\mathrm{peak}} > 0.1\,\mathrm{TW}$ can be attained and utilized for warm-dense

#193989 - $15.00 USD Received 17 Jul 2013; revised 17 Sep 2013; accepted 2 Oct 2013; published 15 Nov 2013

matter experiments [24]. Finally, a laser system that operates in an FEL environment has to achieve long-term stability, which is indispensable for an uninterrupted operation during FEL user experiments.

In this article, we give an overview about the OPCPA setup and first results of our prototype setup. Using three non-collinear OPCPA stages we attained 1.4 mJ of pulse energy at an intra-burst repetition rate of 27.5 kHz. The amplified bandwidth supported sub-7 fs pulse duration. Furthermore, we present active and passive approaches taken to conceive a long-term stable operation of a high power OPCPA. The active solutions involve balanced optical cross-correlation [25] and spectral measurements. The passive solution is based on continuum generation as broadband source for seeding the OPCPA [26, 27].

2. OPCPA setup and results

The experimental setup of the OPCPA is presented in Fig. 1. As the frontend, a Ti:sapphire oscillator was used (Venteon Pulse:One OPCPA seed), delivering 2.5 nJ pulses at a repetition rate of 108 MHz. All-optically synchronized seeding was realized, because the broad spectral range from 650 nm to 1150 nm was sufficiently large to directly seed the Yb-based pump amplifier at 1030 nm as well as the broadband OPCPA at a center wavelength of 800 nm. The three-stage non-collinear OPCPA consisted of three β-barium borate (BBO) crystals of length 3.3 mm, 3.2 mm and 2.0 mm.

The development of new kW-level pump amplifiers at sub-picosecond pulse durations is required to fulfill the high OPCPA criteria concerning broadband pulses with 1 mJ pulse energy at repetition rates up to 1 MHz. Different Yb-based pump amplifier concepts are under development. The amplifiers of the presented system were operated in a 10 Hz burst-mode with 27.5 kHz intra-burst repetition rate. For the pump CPA, the pulses were stretched to 2.26 ns in an Öffner-type stretcher [28]. The pump amplifier chain consisted of subsequent Yb-based amplifiers. The first was an Yb:glass fiber amplifier, delivering 0.36 mJ at 1030 nm. The second was a 0.5 kW Innoslab amplifier, operated at the same repetition rate. The compressed pulse energy was 13.2 mJ at a pulse duration of 1.39 ps FWHM. A 2 mm BBO was used for the frequency doubling (type I phase-matching, $\theta = 23.4°$). OPCPA pump pulses with 6.8 mJ pulse energy were generated at 515 nm with a conversion efficiency of $\eta_{\mathrm{SHG}} = 51.1\%$. The SHG pump intensity was limited by the B-integral in the OPCPA system. The SHG pulse duration was 983 fs FWHM, measured using an autocorrelator (APE: Pulse Check 50).

In the first OPCPA stage, a 3.3 mm BBO was used. This stage was pumped with a fraction of the pump beam (360 µJ). The pump beam diameter was demagnified to 1 mm (at $1/e^2$ intensity) to reach the pump intensity of 81 GW cm^{-2} within the 3.3 mm BBO. The signal beam diameter was 1.3 mm. The signal pulses were amplified from about 1 nJ to 12 µJ, corresponding to a gain of $g = 1.2 \times 10^4$. The signal beam diameter, after amplification, was 1.1 mm owing to spatial gain narrowing.

A high level of amplified optical parametric fluorescence (AOPF) is expected from the first stage, because of the high gain of $g \approx 10^4$ and the comparably low seed energy of $E_{\mathrm{S}} \approx 1$ nJ. The AOPF can reach a significant intensity, which may be further amplified in the second OPCPA stage [29]. The power contrast between AOPF and OPCPA in the first stage was investigated to evaluate an upper limit for the AOPF that seeds the second OPCPA stage. First, the amplified OPCPA output was measured. For increased statistical relevance, the crystal was pumped in continous-mode at 20 kHz pulse repetition rate (1.6 W at 515 nm) at a pump intensity of 100 GW cm^{-2}. The achieved OPCPA output power was 46 mW (corresponding to $E_{\mathrm{sig}} = 2.3$ µJ pulse energy). Afterwards, the signal beam was blocked, and the AOPF half-cone along the tangential phase-matching direction was measured. The cone was focused onto a calibrated photodiode (Thorlabs DET10A). The measured AOPF energy within the amplified signal area

#193989 - $15.00 USD Received 17 Jul 2013; revised 17 Sep 2013; accepted 2 Oct 2013; published 15 Nov 2013

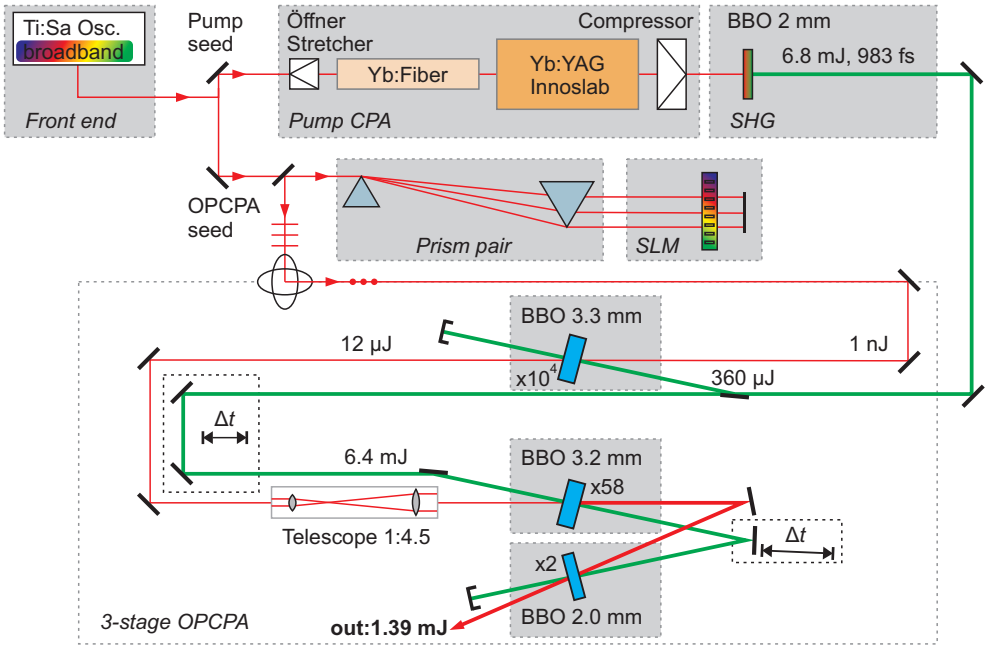

Fig. 1. Schematic of the high power optical parametric chirped-pulse amplifier (OPCPA). The broadband Ti:Sa oscillator seeded the OPCPA and the Yb-based solid-state chirped-pulse amplifier (Pump CPA) that was used for OPCPA pumping. The pump CPA consisted of a 10 W Yb:glass fiber amplifier and a 0.5 kW Yb:YAG Innoslab amplifier. Frequency doubling was achieved in a 2 mm β-barium borate (BBO) crystal. For stretching the OPCPA signal pulses, a prism pair was used. In combination with a spatial light-modulator (SLM), full control of the spectral phase was allowed for the dispersion management of the system. Three subsequent OPCPA stages were implemented, using BBO crystals of 3.3 mm, 3.2 mm and 2.0 mm lengths. The first stage was pumped by a fraction of the SHG output (gain: $g \approx 10^4$). Between the first and the second stage, the amplified signal was magnified by a 1:4.5 telescope. After the third stage, a final output energy of 1.39 mJ is obtained (gain: $g = 58$ in the second stage and $g = 2$ in the third stage)).

was 2.6 nJ. The corresponding AOPF-to-OPCPA energy contrast of $E_{\mathrm{AOPF}}/E_{\mathrm{sig}} \approx 10^{-3}$ represents an upper limit. The AOPF divergence angle was $\theta = 0.5^\circ$. Thus, after a propagation distance of $z = 1.5$ m to the second stage, the AOPF-to-OPCPA intensity contrast was about $I_{\mathrm{AOPF}}/I_{\mathrm{OPCPA}} = (E_{\mathrm{AOPF}}/E_{\mathrm{sig}}) \cdot w_{\mathrm{sig}}^2/(z \tan\Theta)^2 \cdot (\tau_{\mathrm{sig}}/\tau_{\mathrm{AOPF}}) \approx 10^{-5}$. Here, $\tau_{\mathrm{sig}} = 730$ fs is the pulse duration of the signal after the first stage (at $1/e^2$ intensity), and $\tau_{\mathrm{AOPF}} = 1670$ fs pulse duration of the AOPF (at $1/e^2$ intensity), which is assumed to be equal to the pump pulse duration. The AOPF divergence angle was determined by measuring the fluorescence spectrum in dependence on the internal non-collinear angle, α (see Fig. 2(a)). For this measurement, an aperture with 200 µm diameter was moved along α direction within the phase-matching plane. It was mounted onto a multi-mode fiber-bundle coupled to a grating spectrometer (Shamrock SR-303i-B with Andor iDus DV420A-OE detector). From Fig. 2(a), the internal opening angle of the cone, $\Delta\alpha \approx 0.6^\circ$, was obtained, yielding the external divergence angle of $\theta = 0.5^\circ$. With a contrast of $< 10^{-5}$, we expect negligible AOPF from the final amplifier stages, because the AOPF is quenched by the presence of the seed signal.

The second OPCPA stage (a 3.2 mm long BBO crystal) was pumped with 6.4 mJ with a

#193989 - $15.00 USD Received 17 Jul 2013; revised 17 Sep 2013; accepted 2 Oct 2013; published 15 Nov 2013

beam diameter of 3.7 mm (at $1/e^2$ intensity), yielding an intensity of 105 GW cm^{-2}. Between the first and the second stage the signal beam was expanded by a 1:4.5 telescope to a diameter of 5.0 mm. The signal was amplified with a gain of $g = 58$ to a pulse energy of 0.7 mJ, corresponding to a total pump-to-signal conversion efficiency of 10%.

To reach an additional gain of $g = 2$, a third OPCPA stage was implemented. The residual pump from the second stage was used to pump a 2 mm BBO crystal. Efficient energy extraction was achieved by fine-tuning the delay between pump and signal pulses within the second and the third OPCPA stage. A total pulse energy of 1.39 mJ was achieved, corresponding to a final pump-to-signal conversion efficiency of 20%. The efficiency from the compressed Innoslab output at 1030 nm to the OPCPA output was 10%. The overall efficiency was 7.7%, derived from the uncompressed output,

$$17.6\,\mathrm{mJ} \xrightarrow{\text{comp. } 75\%} 13.2\,\mathrm{mJ} \xrightarrow{\text{SHG } 51.1\%} 6.8\,\mathrm{mJ} \xrightarrow{\text{OPCPA } 20\%} 1.4\,\mathrm{mJ}. \tag{1}$$

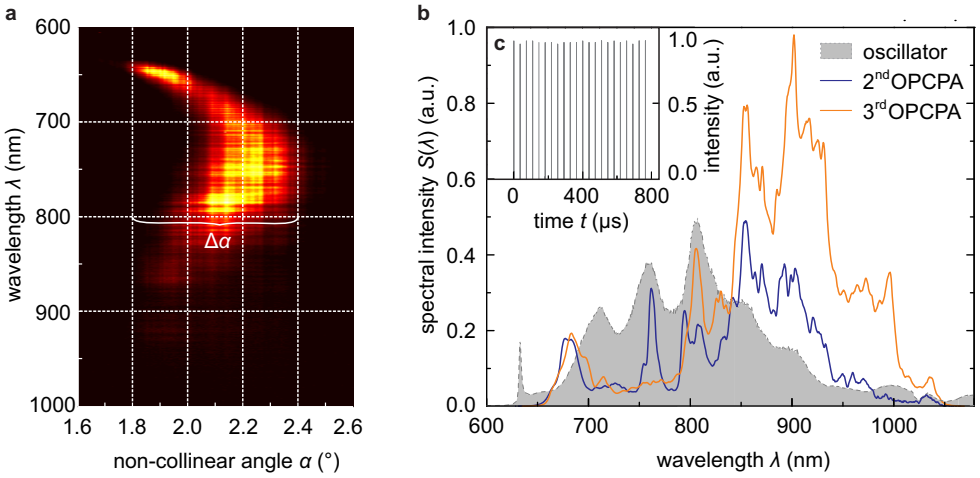

Fig. 2. OPCPA spectral characterization: (a) Spectral intensity of the amplified optical parametric fluorescence (AOPF) at different internal non-collinear angles α. The internal opening angle of the cone was $\Delta\alpha = 0.6°$. (b) Spectral intensity of the Ti:sapphire oscillator (grey shaded), amplified spectra after the second (blue line) and the third OPCPA stage (orange line). The amplified spectral bandwidth is $\Delta\nu = 168$ THz at $1/e^2$ ($\Delta\lambda = 360$ nm at $\lambda_c = 800$ nm), featuring a Fourier-limited pulse duration of 6.4 fs. (c) Inset: Typical pulse train during the burst-mode operation.

In Fig. 2(b), the spectral intensities of the Ti:sapphire oscillator (grey shaded), and of the output of the second (blue line) and third (orange line) OPCPA stage are presented. The amplified bandwidth was $\Delta\nu = 168$ THz at $1/e^2$ ($\Delta\lambda = 360$ nm at $\lambda_c = 800$ nm). Stretching of the signal pulses was achieved by a fused silica prism pair, introducing negative group velocity dispersion, β_2. This negative chirp precompensated the positive β_2 within the OPCPA signal path. The total amount of dispersion introduced by the 8.5 mm of BBO, 10 m of air and 23.6 mm of glass was calculated by expanding the spectral phase around the carrier frequency, $\omega_c = 2.36$ PHz ($\lambda_c = 800$ nm), up to the sixth order: $\varphi(\omega)|_{\omega_c} = \varphi(\omega_c) + \sum_{n=1}^{N=6} \frac{\beta_n}{n!} (\omega - \omega_c)^n + O(n > 6)$, using the dispersion coefficients, $\beta_n = \mathrm{d}^{(n)}\varphi(\omega)/\mathrm{d}\varphi(\omega)^{(n)}|_{\omega_c}$. While the prism pair compensated the β_2, it adds a major contribution to the higher-order coefficients. Consequently, proper pulse compression would be prevented due to the residual uncompensated phases, $\beta_3 = -1911$ fs^3,

#193989 - $15.00 USD Received 17 Jul 2013; revised 17 Sep 2013; accepted 2 Oct 2013; published 15 Nov 2013

$\beta_4 = -11723\,\mathrm{fs}^4$, $\beta_5 = 11285\,\mathrm{fs}^5$ and $\beta_6 = -53615\,\mathrm{fs}^6$. Higher orders, $O(n > 6)$, were neglected. For an accurate phase compensation, a liquid-crystal spatial-light modulator (SLM, Jenoptik SLM-S640) was placed in the focussed Fourier-plane of the prism pair. During the propagation along the signal path, the pulses get gradually compressed. After stretching to about 950 fs (at $1/e^2$ intensity), the calculated pulse duration after the first, second and third OPCPA stage was about 730 fs, 520 fs and 360 fs, respectively. After the third stage, the dispersion of an additional 6 mm fused silica bulk compressor led to a calculated pre-compression of about 170 fs. The final compression can be achieved by a pair of positively chirped mirrors ($\beta_2 = +200\ \mathrm{fs}^2$) in vacuum.

A Fourier-transformation was carried out in order to evaluate the compressible pulse duration. Using the measured spectral amplitude and the phase from the dispersion calculation with different compensated orders of dispersion, the calculation showed that reaching the sub-7 fs regime requires dispersion compensation at least up to the fourth order. The Fourier-limited (FTL) pulse duration yields 6.4 fs FWHM. The Fourier-limited pulse shape is a Gaussian intensity envelope with pedestal (10% pedestal-to-peak contrast). Experimentally, the nonlinear spectral phase added by the OPCPA also needs to be taken into account [30].

In Fig. 2(c) (inset), the typical temporal structure of an amplified burst is shown, recorded with a photodiode (Thorlabs DET10A) and a 2.5 GHz oscilloscope (Tektronix DPO7204). It contains 22 pulses with a pulse energy of 1.39 mJ, resulting in a total burst energy of 30.6 mJ. The stable operation of the three-stage non-collinear OPCPA could only be achieved when the laboratory conditions remained stable. Under stable temperature and humidity conditions, we measured an energy deviation of $\Delta E/E < 0.7\%$ rms over a period of 30 minutes. However, during long-term operation, a considerable drift of the pump-to-seed timing occurred, resulting from a path length change of the pump CPA due to temperature and humidity drift. This could change the average output energy and the spectral bandwidth by up to 50%. The development of pump-to-signal synchronization techniques is thus indispensable for a long-term stable operation.

3. Temporal synchronization techniques

The temporal synchronization between pump and signal pulses is of critical importance in large-scale OPCPA systems. Especially with ultrashort pump pulses in the picosecond range, the OPCPA output power and the spectral bandwidth are sensitive to the temporal overlap between pump and signal pulses. In the presented system, the temporal drift is introduced by thermal changes in the path length of the pump amplifier chain. In Fig. 3, different synchronization approaches are presented. In the active synchronization scheme (Fig. 3(a)), a broadband Ti:sapphire oscillator is used as master oscillator for an all-optically synchronized seeding of the pump CPA and the OPCPA. The occuring delay drift between these two optical paths, Δt, is measured either with a balanced optical cross-correlator (BXC) [25] or by determination of the spectral center of gravity (COG) of the OPCPA output. The Δt-signal is then fed back to a proportional control loop driving an optical delay line in the pump amplifier. In the passive scheme (Fig. 3(b)), a white-light continuum is generated from a fraction of the pump CPA to provide an intrinsically synchronized broadband OPCPA seed. The pump pulses are split after the pump CPA. The BXC is used to study the intrinsic timing jitter originating from the continuum generation process.

To quantify the synchronization sensitivity, we used a two-dimensional OPCPA simulation. The model includes the (z,t)-axis along the signal propagation and the x-axis in transverse direction, both in the phase-matching plane formed by the signal and the pump pulses. The nonlinear coupled wave equations for three-wave mixing are solved for each position using a split-step Fourier algorithm. The system of equations is solved using a fourth-order Runge-

#193989 - $15.00 USD Received 17 Jul 2013; revised 17 Sep 2013; accepted 2 Oct 2013; published 15 Nov 2013

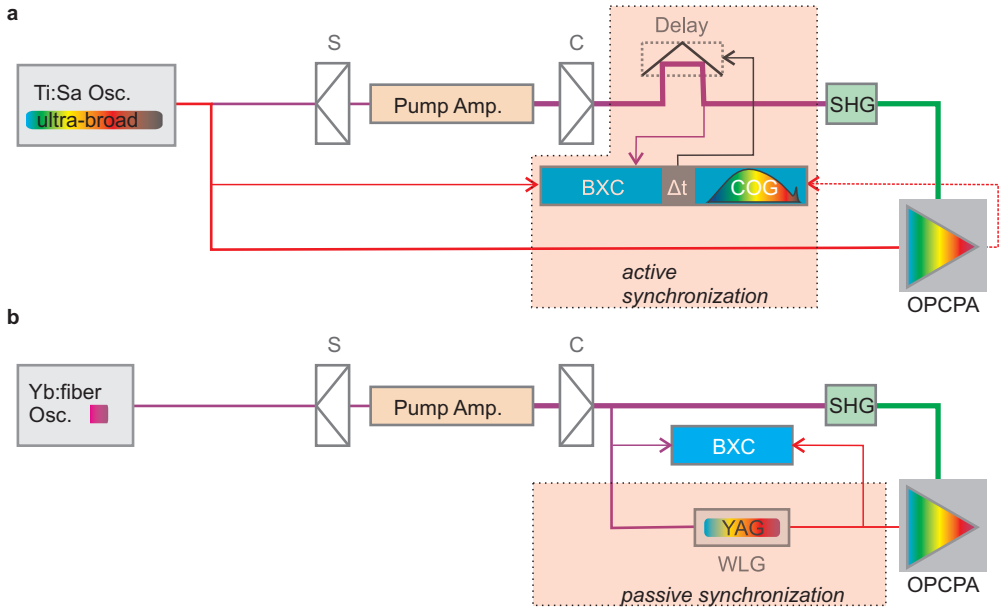

Fig. 3. Synchronization techniques for OPCPA: (a) Schemes for active stabilization with a broadband Ti:sapphire oscillator front end. The setup is similar to the OPCPA setup in section 2. The first synchronization option is to determine the spectral center of gravity (COG) of the amplified OPCPA output (dashed red arrow), which is linearly proportional to the pump-to-signal delay, Δt. The second option is to correlate the compressed pulses from the pump amplifier (purple arrow) and the signal pulses (red arrow) from the oscillator using a balanced optical cross-correlator (BXC). The BXC gives a background free signal, insensitive to intensity fluctuations and linearly proportional to Δt. In both cases, the Δt-signal can be used as a feedback signal to a controlled optical delay line. (b) Scheme for passive stabilization: A fraction of the pump pulses is used for white-light continuum generation (WLG) in a YAG crystal to provide intrinsically synchronized broadband signal pulses for seeding the OPCPA. In this scheme, the broadband oscillator is replaced by an Yb:glass fiber oscillator. The BXC is not required, but it was used to investigate the intrinsic pump-to-signal temporal jitter originating from the WLG process.

#193989 - $15.00 USD Received 17 Jul 2013; revised 17 Sep 2013; accepted 2 Oct 2013; published 15 Nov 2013

Kutta algorithm. Translation of the pump and idler pulses are carried out in the spectral domain, including dispersion and spatial walk-off effects.

The output energy and spectral bandwidth of a non-collinear OPCPA was numerically investigated in dependence on the delay between pump and signal within a range of $\Delta t = \pm 0.4$ ps. The simulation results are presented in Fig. 4. Two different signal spectra were used for the simulation: an experimentally measured spectrum of the Ti:sapphire oscillator (dots) and a broadband Gaussian spectrum (solid lines). Regarding the energy maximum in Fig. 4(a) (dash-dotted vertical line), the delay must be smaller than $|\Delta t| < 50$ fs to not exceed an energy deviation of $\Delta E/\Delta t < 1\%$ (Fig. 4(a)). In Fig. 4(b), the output spectrum was evaluated in terms of its spectral bandwidth (red) and the variation of its center wavelength by means of the center of gravity (COG), λ_{COG}. Within the mentioned ± 50 fs (with respect to the energy maximum), the bandwidth decreases by about 1% of the maximum bandwidth. The central wavelength varies linearly by about 0.2 nm/fs within this range. Consequently, in order to measure and control the pump-to-signal delay within an OPCPA, monitoring the spectral COG represents a suitable solution.

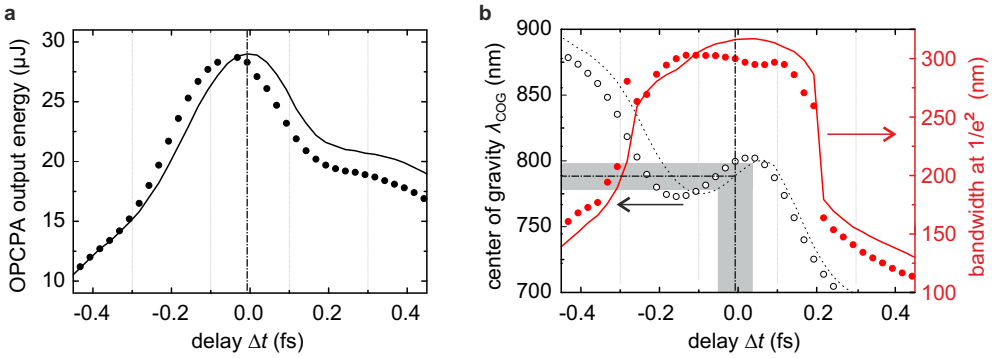

Fig. 4. Numerical simulation of the influence of the temporal delay between pump and signal pulses on the OPCPA, calculated for an experimentally measured broadband seed spectrum (dots) and a broadband Gaussian seed spectrum (lines): (a) Variation of the pulse energy. For a deviation of less than $< 1\%$, the drift must be smaller than < 50 fs with respect to the energy maximum. (b) Amplified spectral bandwidth (red) and central wavelength (center of gravity, black). Within a delay of ± 50 fs with respect to the energy maximum, the spectral bandwidth varies about 1%. The central wavelength varies linearly by about ± 10 nm (grey region). Thus, determining the COG of the OPCPA output spectrum provides a suitable method to measure and control the temporal pump-to-signal drift.

Experimentally, a two-crystal BXC was used to measure the temporal delay between pump and signal pulses. Simultaneously, the output energy and the spectrum of a fiber-pumped non-collinear OPCPA was measured. The BXC consisted of two individual cross-correlators, where the sum-frequency ($\lambda_3 = 417$ nm) of the fundamental pump pulses ($\lambda_2 = 1030$ nm) and the signal pulses ($\lambda_1 = 700$ nm) was generated in 1 mm BBO crystals with type-I phase-matching ($\Theta = 27.7°$). The sum-frequency signal of each correlator was measured with a photomultiplier (Hamamatsu H6780). For the balanced detection, a group delay between pump and signal pulses was introduced in one of the correlator arms by using a 6 mm fused silica plate. Measuring the difference voltage between both detector signals yielded a background-free signal, which was insensitive to intensity fluctuations within the single correlator arms. The signal was proportional to the temporal delay in direction (sign) and amplitude. Thus, it was used as a feedback signal for active pump-to-signal synchronization.

#193989 - $15.00 USD Received 17 Jul 2013; revised 17 Sep 2013; accepted 2 Oct 2013; published 15 Nov 2013

The OPCPA output power and the amplified spectral density were measured over a period of 60 minutes, whilst the temporal delay was recorded using the BXC. First, the OPCPA was operated without the feedback loop activated. Because we expected drifts larger than ± 50 fs, the signal pulses were overstretched to achieve a higher sensitivity of the output spectrum on the pump-to-signal delay. The center wavelength was tuned to 730 nm. A temporal drift between $+400$ fs and -200 fs was observed, corresponding to a decrease of the OPCPA output power of about 22%. In Fig. 5(a), the deviation of the calculated spectral COG, $\Delta\lambda_c = \lambda_{COG} - \lambda_c$, from the central wavelength, $\lambda_c = 730$ nm, was calculated and correlated with the measured drift (red dots). Within a range of ± 200 fs (blue region), the COG varies linearly by $\Delta\lambda_c/\Delta t = -15.76 \pm 0.16$ nm/ps (black line). Compared to the simulation (± 50 fs linear range), the linear range was extended by the stretching. As shown in Fig. 3(a) (red dashed OPCPA output), the spectral COG can be directly used to proportionally measure and control the pump-to-signal drift in an OPCPA.

The delay measurement was repeated with the BXC feedback loop activated. In this case, no long-term drift of the temporal delay and no drift of the OPCPA output power or the spectral bandwidth was observed. However, a residual timing jitter of $\delta t = (46 \pm 2)$ fs rms was measured. The corresponding OPCPA power jitter was $\delta P/P = 1.2\%$ rms. This remaining jitter is larger compared to the jitter of the three-stage OPCPA presented in section 2. In general, we expect a higher jitter from the single-stage amplifier, because it was operated in the small-signal gain regime, where the output is more sensitive to fluctuations of the pump energy. The high power stages were operated in the saturated gain regime with less sensitivity. However, additional jitter is also expected to originate from the noise of the applied analog-to-digital converters and the proportional control loop. To minimize this jitter further, low-noise electronics should be used for the measurement and control system. To further optimize the control, a fast proportional-integral-derivative (PID) controller should be used in combination with an additional fast piezo actuator in the delay line [20]. In this way, the pump-to-signal jitter could be reduced to 18 fs rms in a high repetition rate fiber-pumped OPCPA [31].

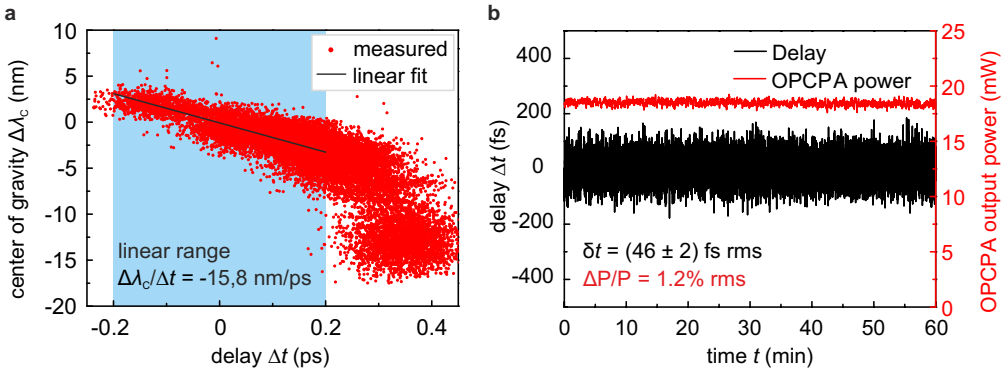

Fig. 5. Pump-to-seed synchronization of an OPCPA: (a) Variation of the center of gravity (COG) wavelength, $\Delta\lambda_C$, of the unstabilized OPCPA spectral intensity (red dots) in dependence on the delay measured with a balanced optical cross-correlator (BXC). Within a range of ± 0.2 ps (blue region), the COG varies linearly by $\Delta\lambda_C/\Delta t = -15.76 \pm 0.16$ nm/ps (black line). (b) Temporal delay (black) and output power (red) of an actively stabilized OPCPA, measured over 60 minutes. The delay is measured and controlled using the in-loop BXC signal as feedback to an optical delay line. The residual timing jitter is $\delta t = (46 \pm 2)$ fs rms, the corresponding jitter of the output power is 1.2% rms.

In the passive synchronization approach, broadband OPCPA seed pulses are directly generated

#193989 - $15.00 USD Received 17 Jul 2013; revised 17 Sep 2013; accepted 2 Oct 2013; published 15 Nov 2013

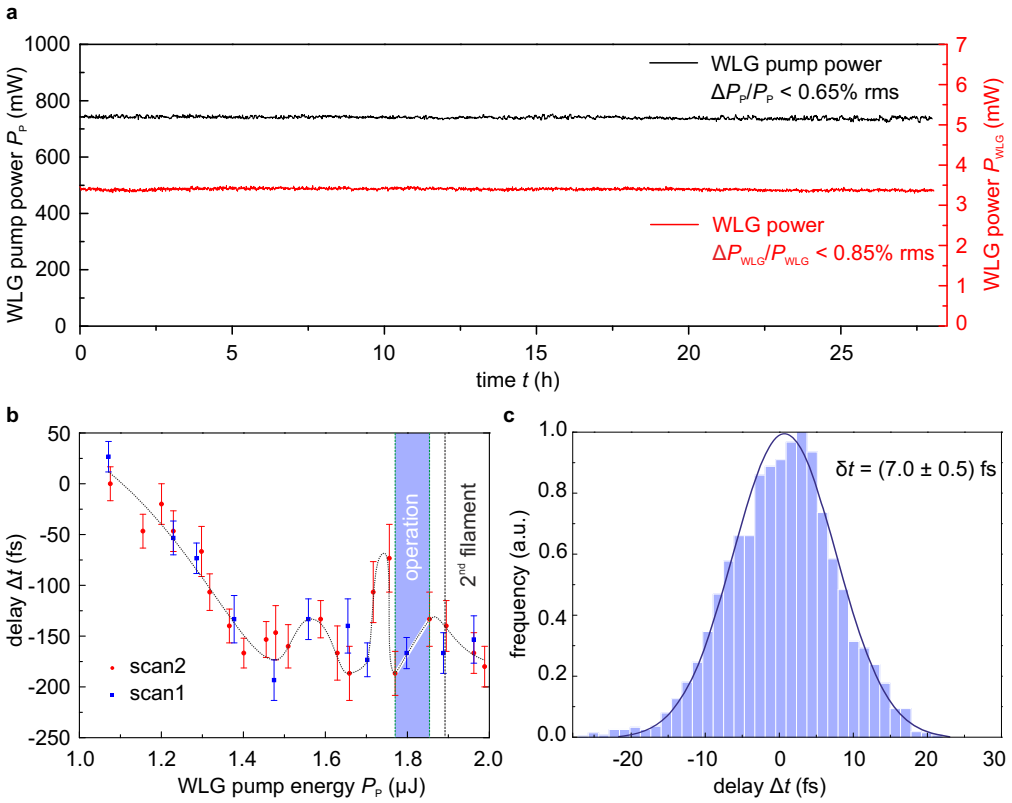

Fig. 6. Passive synchronization by white-light continuum generation (WLG). (a) Pump power (black) and WLG power (red), measured over 28 hours. The power deviation is smaller than $< 0.65\%$ rms for the pump and $< 0.85\%$ rms for the WLG power. The investigated WLG spectral region ranged from 650 nm to 950 nm. (b) Delay between pump and WLG pulses at different pump pulse energies, measured with a BXC. The blue region indicates the operation regime (about 1.8 μJ). Above 1.9 μJ a second WLG pulse is generated (dashed line). Within the operation regime, the delay varied with a slope of $\Delta T/\Delta P_\mathrm{P} = (0.66 \pm 0.04)\,\mathrm{fs/nJ}$. (c) Pump-to-WLG delay jitter, derived from the pump jitter in (a) and the slope from the operation regime in (b), $\Delta t = P_\mathrm{P}(t) \cdot \Delta T/\Delta P_\mathrm{P}$. The rms width is $\delta t = (7.0 \pm 0.5)\,\mathrm{fs}$.

#193989 - $15.00 USD Received 17 Jul 2013; revised 17 Sep 2013; accepted 2 Oct 2013; published 15 Nov 2013

from a fraction of the compressed sub-ps pump pulses. In this way, the path length of the pump and the signal pulses is reduced to a minimum (about 2-4 m). For the broadband signal generation, white-light continuum generation (WLG) in a YAG crystal is the most promising method [26]. Using this technique, first OPCPAs have already been successfully demonstrated [14, 27]. As illustrated schematically in Fig. 3(b), a 20 W Yb:glass fiber amplifier was used as the pump amplifier. The system delivered pulse durations down to 333 fs at repetition rates tunable from 20 kHz to 4 MHz. About 1.8 µJ of pulse energy was required to achieve stable white-light continuum generation in a YAG crystal. For the optimum WLG stability, a crystal length of 5 mm was chosen. The pump pulses were focussed into the crystal with a lens of $f = 50$ mm and a numerical aperture of $NA \approx 0.02$. The focal point was placed close to the input surface within the crystal. The WLG spectrum ranged from about 480 nm to beyond 1500 nm. For the OPCPA seed characterization, a part of the spectrum (650 nm to 950 nm) was selected by use of dichroic mirrors.

It was of particular interest whether the WLG process itself introduced a timing jitter at a given pump laser energy stability. With increasing pump energy, the position of the filament shifts towards the input surface of the crystal [32, 33]. The threshold power for self-focussing varies for a higher pump energy and thus the onset of filamentation shifts towards the rising edge of the intensity envelope of the pump pulse, introducing a pump-to-signal delay. Additionally, for different filament positions the group delay (GD) between pump and WLG pulses varies due to different optical paths, z, within the YAG crystal. The GD varies about $\Delta GD/\Delta z \approx 40\,\mathrm{fs/mm}$. First, the power stability of the fiber laser and the selected WLG output was measured over a period of 28 hours. As shown in Fig. 6(a). the fiber laser stability was $\Delta P_\mathrm{P}/P_\mathrm{P} = 0.65\%$ rms and 4.1% maximum deviation (black line, measured with calibrated Thorlabs DET10A photodiode). On a pulse-to-pulse basis, the maximum deviation was less than 1.2%. No significant drift of the WLG output power was measured (red line). The WLG power jitter was $\Delta P_\mathrm{WLG}/P_\mathrm{WLG} = 0.85\%$ (Ophir 3A power meter). Thereafter, the intrinsic temporal jitter between WLG pump and WLG pulses was studied using the BXC. For that purpose, a fraction of the 1030 nm pump pulses was correlated with a spectrally filtered (650 ± 10) nm part of the WLG pulses in the BXC. The sum-frequency signal of the BXC was at 399 nm. The measurement is presented in Fig. 6(b). The onset of WLG was observed at pump energies of $E_\mathrm{P} \geq 1$ µJ. In this case, the position of the filament was at the end of the crystal. By increasing the pump energy to 1.47 µJ, an increase of the delay between pump and WLG of about 200 fs was measured. Further increase of the pump energy led to an oscillation of the delay. This is attributed to a sequence of plasma-defocussing and re-focussing due to self-focussing of a fraction of the pulse energy that is not coupled into the filament. Above a pump pulse energy of 1.9 µJ, the pump energy was sufficient to form a second filament and thus a second WLG pulse. This pulse is delayed by about 160 fs with respect to the first WLG pulse, leading to stable interference modulations in the WLG spectrum.

The operation point for the stable generation of single WLG pulses was chosen slightly below the onset of the second filament at $E_\mathrm{P} \approx 1.8$ µJ, as indicated by the blue region in Fig. 6(b). The delay within this region varies by $\Delta T/\Delta E_\mathrm{P} = (0.66 \pm 0.4)\,\mathrm{fs/nJ}$. Applying this variation to the jitter of the pump energy from Fig. 6(a) provides a good estimate of the intrinsic timing jitter of the continuum seeder (Fig. 6(c)), yielding $\delta t = (7.0 \pm 0.5)$ fs rms (16 fs FWHM).

4. Conclusion

We developed a high power burst-mode OPCPA for applications at the free-electron laser FLASH. Three non-collinear OPCPA stages were operated with an intra-burst repetition rate of 27.5 kHz (22 pulses in a 800µs burst), pumped by sub-picosecond pulses from an Yb:YAG Innoslab amplifier. We achieved 1.4 mJ pulse energy and an amplified spectral bandwidth sup-

#193989 - $15.00 USD Received 17 Jul 2013; revised 17 Sep 2013; accepted 2 Oct 2013; published 15 Nov 2013

porting sub-7 fs pulse duration. Under stable laboratory conditions, the stable operation over a period of 30 minutes was demonstrated with an energy deviation of $\Delta E/E < 0.7\%$ rms. For long-term operation, temperature drifts and slow humidity changes caused a critical drift of the pump-to-signal temporal overlap in the OPCPA. This results in a 50% decrease of the output energy and the spectral bandwidth. These critical parameters were investigated numerically and experimentally.

Furthermore, active and passive pump-to-signal synchronization techniques were investigated. We performed numerical calculations to study the influence of the pump-to-signal delay in an OPCPA. Aiming for a jitter of the amplified average energy of less than 1% rms, a pump-to-signal delay $|\Delta t| < 50$ fs was estimated. Within this temporal window, a variation of the spectral bandwidth of about 1% can be expected (at $1/e^2$ spectral intensity). For testing active synchronization schemes, we measured the pump-to-signal drift in a single OPCPA stage using a balanced optical cross-correlator (BXC). In these mesaurements, we observed a slow temporal drift of about $+400$ fs to -200 fs during a period of 1 hour. Investigating the center of gravity of the OPCPA output spectrum, we found experimentally and numerically that the center wavelength varied linearly with the temporal delay within the required synchronization window. Accordingly, we suggest to use this signal for drift compensation in OPCPAs. Furthermore, we implemented a feedback of the BXC timing signal to an optical delay line. Employing a motor-driven linear translation stage, we achieved a drift-free OPCPA operation with a residual pump-to-seed jitter of $\delta t < 46$ fs rms, corresponding to an energy jitter of 1.2% rms, measured over a period of 1 hour. To optimize the performance, low noise photodiodes and a fast proportional-integral-derivative controller in combination with fast piezo actuators should be used. For a passive stabilization, intrinsically synchronized broadband OPCPA seed pulses were derived from the pump pulses by white-light continuum generation (WLG) in YAG. Using a stable Yb:glass fiber amplifier as pump, a WLG energy deviation of less than 0.85% rms was achieved (650 nm - 950 nm), measured over a period of 28 hours. After one day of operation, no decrease of the WLG signal was observed. Investigation of the intrinsic timing jitter originating from the white-light generation yielded $\delta t = 7$ fs rms, derived from a BXC measurement.

For increasing the long-term stability of high power OPCPAs, the implementation of either active or passive synchronization systems is indispensable. Using the presented active methods, we successfully demonstrated a drift-free OPCPA operation. The method of choice depends on the demanded OPCPA seed parameters. WLG pulses offer a larger spectral bandwidth in the visible. On the other hand, the available Ti:sapphire oscillators offer the possibility for carrier-envelope phase stabilization, which has not been shown so far for WLG pulses. Furthermore, the energy stability of available broadband Ti:sapphire oscillators ($< 0.1\%$ rms) has not been reached using WLG. However, passive synchronization intrinsically reaches few-fs resolution, whereas active techniques require additional implementation of optical, mechanical and electronic devices.

With upcoming kW-class Yb-based solid-state amplifier technologies, OPCPA pump amplifiers will soon be available to operate the presented high power OPCPA at repetition rates of 100 kHz up to 1 MHz with mJ-level pulse energies and sub-10 fs pulse durations. The progress of these techniques represents a major development step in femtosecond laser technology.

Acknowledgments

We thank the team of the Photon Science department of Deutsches Elektronensynchrotron DESY in Hamburg.

#193989 - $15.00 USD Received 17 Jul 2013; revised 17 Sep 2013; accepted 2 Oct 2013; published 15 Nov 2013